J. Fluid Mech. (1992), *vol.* 234, *pp.* 417–441
Printed in Great Britain

On the resonant triad interaction in flows over rigid and flexible boundaries

By MICHAEL D. THOMAS
Department of Mathematics, University of Exeter, Exeter EX4 4QE, UK†

(Received 27 September 1990 and in revised form 1 July 1991)

Resonant interactions in flows over rigid and flexible walls are studied. Attention is concentrated on symmetric, three-dimensional wave triads as proposed by Craik (1971). Location of resonant triads and evaluation of interaction coefficients are performed numerically, for a wide range of Reynolds numbers and wavenumbers, considering the temporal stability problem. Good agreement is found with previous work. It is shown that triads comprising various combinations of Tollmien–Schlichting and/or wall modes are possible, and have some interesting features; also, the possibility of interaction with Squire modes must not be overlooked.

1. Introduction

The linear stability of flows over flexible boundaries has been comprehensively studied in recent years (see for example Carpenter & Garrad 1985, 1986; Yeo 1986; Carpenter 1990). The main purpose of these analyses has been to try and determine the extent to which flexible walls are capable of delaying transition from laminar to turbulent flow, and of reducing drag on marine craft. Many of the experiments that have been performed (e.g. those of Gad-el-Hak, Blackwelder & Riley 1984) strongly indicate that three-dimensionality (and hence perhaps nonlinearity) is even more prominent than for rigid-wall flows. Also, the multiplicity of modes in flexible-wall flows suggests that nonlinear modal interaction (in the form of resonant triads, for example) may often be of importance, especially when there is no linear mode coupling. Despite this, there has as yet been little theoretical work on the nonlinear stability problem, although Rotenberry & Saffman (1990) have studied the effect of compliant walls on the weakly nonlinear stability of plane Poiseuille flow.

We shall focus on resonant triad interactions of the type proposed by Raetz (1959), which were subsequently studied by Craik (1971). Such interactions are important because in many instances they will be the first nonlinear flow modification to occur, being $O(A^2)$ phenomena rather than $O(A^3)$ as is more generally the case (A is a characteristic wave amplitude). Previous work on rigid-wall flows (Usher & Craik 1974, 1975; Volodin & Zel'man 1979) has shown that oblique modes are preferentially amplified by the resonant triad interaction, and this may often account for the rise of three-dimensionality in the laminar–turbulent flow transition process. Indeed, the experiments of Kachanov & Levchenko (1984), and others, provide some support for this viewpoint.

The parametric subharmonic mechanism of Herbert (1983, 1988) is related to the Craik mechanism, but the precise nature of the relationship is a little unclear. Experiments (Saric & Thomas 1984) indicate that the Herbert (or 'H-type')

† Present address: Department of Engineering, University of Warwick, Coventry CV4 7AL, UK.

mechanism requires slightly higher initial amplitudes than that of Craik ('C-type') in order to occur. The elegance and simplicity of the C-type resonant triads make them eminently suitable, we believe, for our preliminary study of nonlinear stability of flows over flexible walls.

In this work we consider Blasius flows over a simple model wall. Temporal eigenvalues of the Orr–Sommerfeld (OS) equation, resonant triads and interaction coefficients are found by numerical integration. Parallel flow is assumed throughout the Blasius solution is in fact only 'nearly parallel'. Previous work (for example Smith 1979) has shown that parallel and non-parallel theories give broadly similar results, the major discrepancy being an extension to the tip of the neutral curve, which gives improved agreement with experiment. Temporal wave modes are investigated in preference to spatial ones chiefly because they present a slightly more tractable numerical task.

Our simple wall model is representative of a membrane supported by springs:

$$N = m\frac{\partial^2 \eta}{\partial t^2} + d\frac{\partial \eta}{\partial t} - F\nabla^2\eta + S\eta, \tag{1a}$$

such as was used by Benjamin (1963). In (1a) N is the normal stress at the fluid–solid interface, η is the vertical displacement, and $\boldsymbol{\nabla} \equiv \partial/\partial x\boldsymbol{i} + \partial/\partial y\boldsymbol{j}$. In our chosen coordinate frame x, y and z denote the streamwise, transverse and normal directions respectively. It is assumed that there is no lateral wall motion. The parameters may be assigned particular physical identities, for example those characteristic of a stretched membrane: m would then be the effective membrane mass per unit area, d a damping coefficient due to viscous or frictional effects, F the tension per unit span of the membrane and S its effective spring stiffness.

In practice, the compliant material may well be of complex construction. The 'Kramer surfaces' discussed by Carpenter & Garrad (1985), for example, consisted of a layer of pliable rubber-like material supported on a rigid base by an array of closely spaced flexible stubs, with viscous fluid in the gap between them. Detailed mathematical analysis of such composite materials is impracticable, and so they are best represented by judicious choice of parameters in models like that just introduced. Usually, however, the effective mass, stiffness and so on will not be constants, but will depend on the lengthscale of the disturbance. Accordingly, it is best to replace (1a) by a corresponding representation of the stress $N(\boldsymbol{k})$ associated with each individual Fourier mode $\zeta(\boldsymbol{k})$, proportional to $\exp(\mathrm{i}\boldsymbol{k}\cdot\boldsymbol{x} - \mathrm{i}\omega t)$, with real wavenumber $\boldsymbol{k}$ and (perhaps complex) frequency $\omega(\boldsymbol{k})$; namely

$$N(\boldsymbol{k}) = [-m\omega^2 - \mathrm{i}d\omega + Q]\,\zeta, \tag{1b}$$

where Q is the restoring force and m, d (and perhaps S) are permitted to be prescribed functions of $k = |\boldsymbol{k}|$. We shall assume, for simplicity, that m, d and S are constants, but Q will be given by $Q = Tk^2 + S$, where $T = F\cos\theta$, θ being the angle between the direction of wave propagation and the basic flow. The Fourier-mode representation is discussed in more detail by Thomas & Craik (1988).

Despite our concern with a nonlinear problem, the stress representations (1a) or (b) are linear ones in the wave elevation η or its individual Fourier components. This representation may be altered by additional nonlinear terms – see Thomas & Craik (1988). For present purposes it is advantageous to restrict the number of independent wall parameters while retaining a reasonable degree of realism. More complex models may be examined by similar methods, if required.

All quantities, including those pertaining to oblique modes, are non-dimensionalized using appropriate combinations of U_∞, ρ_e and the boundary-layer thickness δ, which we define to be $\delta \equiv 5(\nu x/U_\infty)^{\frac{1}{2}}$. The Reynolds number R is defined with respect to δ, i.e. $R \equiv U_\infty \delta/\nu$. The wall parameters are non-dimensionalized in the following way:

$$m = \frac{m_*}{\rho_e \delta}, \quad c_0^2 = \frac{c_{0*}^2}{U_\infty^2}, \quad d = \frac{d_*}{\rho_e U_\infty}, \quad S = \frac{S_* \delta}{\rho_e U_\infty^2}, \tag{2}$$

where $c_0^2 \equiv m^{-1}F$ and an asterisk denotes dimensional quantities. This scheme is akin to that of Domaradzki & Metcalfe (1987). R can be taken to vary with δ, U_∞ or ν: here we assume that U_∞ and ν are fixed, and R varies only as δ changes, that is, with x. If allowance is not made for this, different walls will be modelled at different Reynolds numbers. Thus we define reference values $m^{(0)}$ of m and $S^{(0)}$ of S at some Reynolds number R_0, and m and S vary according to

$$m = \frac{m^{(0)} R_0}{R}, \quad S = \frac{S^{(0)} R}{R_0}. \tag{3}$$

Note that R may alternatively be taken to be a function of U_∞ rather than of δ.

2. The linear problem

Here we consider two-dimensional disturbances only. The basic flow $\bar{u} \equiv U(z)/U_\infty$ is assumed to be parallel, satisfying the Blasius equation

$$f''' + ff'' = 0, \tag{4}$$

where $f'(\chi) = \bar{u}(z)$ and $\chi \equiv (5/\sqrt{2})z$; primes here denote differentiation with respect to χ. Boundary conditions are

$$f(0) = f'(0) = 0, \quad f'(\chi) \to 1 \quad \text{as} \quad \chi \to \infty, \tag{5a, b, c}$$

corresponding to the physical requirements that the flow should be stationary at the wall and reach some constant value at a certain distance from the wall. A stream function Φ is defined by $u = \partial\Phi/\partial z$, $w = \partial\Phi/\partial x$. We consider arbitrary small disturbances of the form $\Phi_p = \epsilon\phi(z)\exp(\mathrm{i}\alpha x - \mathrm{i}\alpha c t)$, $\epsilon \ll 1$, and substitute for the total stream function $\Phi = \int \bar{u}\,\mathrm{d}z + \Phi_p$ into the vorticity equation

$$\frac{\partial \nabla^2 \Phi}{\partial t} + \frac{\partial \Phi}{\partial y}\frac{\partial \nabla^2 \Phi}{\partial x} - \frac{\partial \Phi}{\partial x}\frac{\partial \nabla^2 \Phi}{\partial y} - \frac{1}{R}\nabla^4 \Phi = 0. \tag{6}$$

On neglecting $O(\epsilon^2)$ quantities, this yields the OS equation:

$$L[\phi] \equiv \mathrm{i}\alpha[(\bar{u}-c)(\phi'' - \alpha^2\phi) - \bar{u}''\phi] - 1/R(\phi'''' - 2\alpha^2\phi'' + \alpha^4\phi) = 0. \tag{7}$$

The boundary conditions for (7) are, in terms of the perturbation velocities:

$$u(\eta) = 0, \quad w(\eta) = (\partial/\partial t + \boldsymbol{u}\cdot\boldsymbol{\nabla})\eta; \quad u, w \to 0 \quad \text{as} \quad z \to \infty. \tag{8a–d}$$

These correspond to requirements of no slip at the wall, and zero perturbation velocities far outside the boundary layer. Performing Taylor expansions of the first two about the undisturbed wall position yields at first order

$$\phi'(0) + \eta\bar{u}'(0) = 0, \tag{9}$$

$$\phi(0) - c\eta = 0. \tag{10}$$

Elimination of η gives the homogeneous condition

$$\phi'(0)+\frac{\bar{u}'(0)}{c}\phi(0)=0. \tag{11}$$

We require one other boundary condition at the wall, and this is obtained from a consideration of the normal stress:

$$\left[-p+\frac{2}{R}\frac{\partial w}{\partial z}\right]_{z=\eta}=N(\eta). \tag{12}$$

From the x-momentum equation

$$\frac{\partial u}{\partial t}+\boldsymbol{u}\cdot\boldsymbol{\nabla}u=-\frac{\partial p}{\partial x}+\frac{1}{R}\nabla^2 u, \tag{13}$$

and using (11) we have

$$p(0)=\frac{1}{\mathrm{i}\alpha R}(\phi'''(0)-\alpha^2\phi'(0)). \tag{14}$$

The quantity $N(\eta)$ is as given in (1a), with appropriate notational changes. From (1a), (10), (12) and (14) we obtain

$$\phi'''(0)-3\alpha^2\phi'(0)-B\phi(0)=0, \tag{15}$$

where

$$B\equiv\frac{\mathrm{i}\alpha R}{c}[m\alpha^2(c^2-c_0^2)+\mathrm{i}\alpha cd-S]. \tag{16}$$

The free-stream boundary conditions in terms of ϕ are

$$\phi(z),\phi'(z)\to 0 \quad \text{as} \quad z\to\infty. \tag{17a, b}$$

Equation (7) together with the boundary conditions (11), (15) and (17) constitute an eigenvalue problem for $c(\alpha,R)$.

For the rigid-wall case, (17) is unchanged but (11) and (15) are replaced by $\phi(0)=\phi'(0)=0$ (since $u(0)=w(0)=0$).

3. The nonlinear problem: resonant triads

The formulation of the resonant-triad problem for flow over a flexible boundary is a reasonably straightforward extension of that for rigid walls given elsewhere (Craik 1971): however, care must be taken in deriving the wall boundary conditions for the adjoint system, since these cannot be obtained from any physical considerations. Hence the analysis will be given in detail. We consider a triad of waves defined by

$$\boldsymbol{\Phi}_j=\sum_{i=1}^{\infty}[\epsilon^i\phi_j^{(i)}(z)A_j^{(i)}(t)]E_j, \quad j=1,2,3, \tag{18}$$

where

$$\left.\begin{aligned}E_1&=\exp\{\mathrm{i}(\tfrac{1}{2}\alpha x+\beta y-\tfrac{1}{2}\alpha\tilde{c}t)\},\\ E_2&=\exp\{\mathrm{i}(\tfrac{1}{2}\alpha-x-\beta y-\tfrac{1}{2}\alpha\tilde{c}t)\},\\ E_3&=\exp\{\mathrm{i}(\alpha x-\alpha ct)\}.\end{aligned}\right\} \tag{19}$$

Exact resonance requires that $\tilde{c}_r=c_r$. An ordering parameter ϵ has been introduced, so that all perturbation quantities are $O(\epsilon)$ with $o(\epsilon)$ corrections. The amplitudes are

assumed to be slowly varying on a stretched timescale $\tau = \epsilon t$. It is convenient to write (cf. Craik 1971)

$$u_{1,2} = \alpha/2\gamma\,\hat{u}_{1,2} \mp \beta/\gamma\,\hat{v}_{1,2}, \quad v_{1,2} = \pm\beta/\gamma\,\hat{u}_{1,2} + \alpha/2\gamma\,\hat{v}_{1,2}, \tag{20}$$

where $\gamma = (\frac{1}{4}\alpha^2+\beta^2)^{\frac{1}{2}}$. The velocities $\hat{u}_{1,2}$, $\hat{v}_{1,2}$ are defined in the directions $\hat{x}_{1,2}$, $\hat{y}_{1,2}$, which are respectively perpendicular and parallel to the crests of the relevant oblique wave:

$$\hat{x}_{1,2} = \alpha/2\gamma\,x \pm \beta/\gamma\,y, \quad \hat{y}_{1,2} = \mp\beta/\gamma x + \alpha/2\gamma\,y. \tag{21}$$

From the definitions (18) and (19) it follows that

$$\hat{u}_{1,2} = \sum_{i=1}^{\infty} [\epsilon^i \phi_j^{(i)'}(z)\, A_j^{(i)}(t)]\, E_{1,2}, \qquad w_{1,2} = -\mathrm{i}\gamma \sum_{i=1}^{\infty} [\epsilon^i \phi_j^{(i)}(z)\, A_j^{(i)}(t)]\, E_{1,2}. \tag{22}$$

The linearized vorticity equation for the 3-wave gives the OS equation

$$L_3[\phi_3] \equiv \mathrm{i}\alpha[(\bar{u}-c)(\phi_3''-\alpha^2\phi_3) - \bar{u}''\phi_3] - 1/R\,(\phi_3''''-2\alpha^2\phi_3''+\alpha^4\phi_3) = 0, \tag{23}$$

where $\phi_3 \equiv \phi_3^{(1)}$. We now define an oblique Reynolds number $\tilde{R}$ by

$$\tilde{R} \equiv \alpha R/2\gamma, \tag{24}$$

giving for the 1-wave and 2-wave equations equivalent to (23)

$$L_{1,2}[\phi_{1,2}] \equiv \mathrm{i}\gamma[(\bar{u}-\tilde{c})(\phi_{1,2}''-\gamma^2\phi_{1,2}) - \bar{u}''\phi_{1,2}] - 1/\tilde{R}\,(\phi_{1,2}''''-2\gamma^2\phi_{1,2}''+\gamma^4\phi_{1,2}) = 0, \tag{25}$$

where $\phi_{1,2} \equiv \Phi_{1,2}^{(1)}$. Equations (20) and (24) constitute a Squire transformation (Squire 1933).

The linearized momentum equations in the $\hat{y}_{1,2}$ directions yield

$$\hat{v}_{1,2}''-[\gamma^2+\mathrm{i}\gamma\tilde{R}(\bar{u}-\tilde{c})]\,\hat{v}_{1,2} = \pm\mathrm{i}\beta R\bar{u}'\phi_{1,2}. \tag{26}$$

The velocity components $\hat{v}_{1,2}$ arise because of the distorting influence of the basic shear flow on oblique wave modes. The boundary conditions for (23) are just (11), (15) and (17) with appropriate quantities subscripted by 3. For (25), however, the wall boundary conditions depend critically on the type of wall being modelled. In this work we shall consider an idealized orthotropic wall: the effective wall tension experienced by obliquely propagating wall modes is assumed to be $F\cos\theta$ (that is, $(\alpha/2\gamma)F$) rather than just F; θ is the angle between the directions of propagation of the oblique wave and the basic flow. More complicated anisotropic models are of course possible, and indeed have been investigated elsewhere in the context of the linear stability problem (for example Yeo 1986; Carpenter & Morris 1990), but our simple model is appropriate for this exploratory study. At $O(\epsilon)$ we have for the 1-wave

$$\phi_1'(0) = -\alpha/2\gamma\,\bar{u}_0'(0)\eta_1, \tag{27}$$

$$\phi_1(0) = \alpha/2\gamma\,\tilde{c}\eta_1, \tag{28}$$

which gives

$$\phi_1'(0) + \bar{u}'/\tilde{c}\,(0)\,\phi_1(0) = 0. \tag{29}$$

The normal stress is

$$\left[-p_1 + \frac{2}{R}\frac{\partial w_1}{\partial z}\right]_{z=\eta} = N_1(\eta), \tag{30}$$

and the x-momentum equation

$$\frac{\partial u}{\partial t} + \boldsymbol{u}\cdot\boldsymbol{\nabla}u = -\frac{\partial p}{\partial x} + \frac{1}{R}\nabla^2 u \tag{31}$$

yields $$p_1(0) = \frac{1}{\mathrm{i}\gamma R}(\phi_1'''(0) - \gamma^2\phi_1'(0)). \tag{32}$$

Thus we obtain the second wall boundary condition as

$$\phi_1'''(0) - 3\gamma^2\phi_1'(0) - B_1\phi_1(0) = 0, \tag{33}$$

where $$B_1 \equiv \frac{2\mathrm{i}\gamma^2}{\alpha\tilde{c}}\left[\frac{m\alpha^2}{4}\left(\tilde{c}^2 - \frac{\alpha}{2\gamma}c_0^2\right) + \mathrm{i}\frac{\alpha\tilde{c}}{2}d - S\right]. \tag{34}$$

Note that in (30)–(34) the Reynolds number is the original one, not that defined by (24). This can be verified by rederiving the boundary condition in dimensional units, and then non-dimensionalizing according to the scheme given above. The two boundary conditions for (26) are

$$\hat{v}_{1,2}(0) = \pm\beta/\gamma\,\bar{u}'(0)\eta_{1,2}, \tag{35}$$

$$\hat{v}_{1,2}(z) \to 0 \quad \text{as} \quad z \to \infty. \tag{36}$$

The first of these results from the requirement that tangential velocity be zero at the wall, and the second follows on observing that $\bar{u} = 1$ outside the boundary layer. As was found by Craik (1971), at $O(\epsilon^2)$ the nonlinear vorticity equations are

$$\left.\begin{aligned} A_3(t)L_3[\bar{\phi}_3] &= -\frac{\mathrm{d}A_3}{\mathrm{d}\tau}(\phi_3'' - \alpha^2\phi_3) + F_3 \equiv r^{(3)}, \\ A_{1,2}(t)L_{1,2}[\bar{\phi}_{1,2}] &= -\frac{\mathrm{d}A_{1,2}}{\mathrm{d}\tau}(\phi_{1,2}'' - \gamma^2\phi_{1,2}) + F_{1,2} \equiv r^{(1,2)}, \end{aligned}\right\} \tag{37}$$

where $\bar{\phi}_j \equiv \phi_j^{(2)}$, $j = 1, 2, 3$, and F_1, F_2, F_3 are bilinear in the first-order disturbance quantities.† In the remainder of this section the index j takes the values $1, 2, 3$, corresponding to the three constituents of the triad. The wall boundary conditions for (37) are found after considerable algebraic manipulation to be

$$\bar{\phi}_j'(0) + \bar{u}'/c_j\,\bar{\phi}_j(0) = \mu_1^{(j)}, \tag{38a}$$

$$\bar{\phi}_j'''(0) - 3k_j^2\bar{\phi}_j'(0) - B_j\bar{\phi}_j(0) = \mu_2^{(j)}, \tag{38b}$$

where the $O(\epsilon^2)$ terms μ_j represent nonlinear forcing† and $k_{1,2} \equiv \gamma$, $k_3 \equiv \alpha$; $c_{1,2} \equiv \tilde{c}$, $c_3 \equiv c$. The three pairs of free-stream boundary conditions are the same as for the linear problem, i.e.

$$\bar{\phi}_j(z), \bar{\phi}_j'(z) \to 0 \quad \text{as} \quad z \to \infty, \quad j = 1, 2, 3. \tag{39a, b}$$

In order to solve (37), we now consider the linear system adjoint to (23) and (25), viz.

$$L_j^\dagger[\psi_j] \equiv \mathrm{i}k_j[(\bar{u} - c_j)\psi_j]'' - \mathrm{i}k_j[k_j^2(\bar{u} - c_j) + \bar{u}'']\psi_j - 1/R_j(\psi_j'''' - 2k_j^2\psi_j'' + k_j^4\psi_j) = 0 \tag{40}$$

(see e.g. Ince 1956, §9.31), where $R_{1,2} \equiv \tilde{R}$ and $R_3 \equiv R$. The expressions $L_j[\phi_j]$ and $L_j^\dagger[\psi_j]$ are related by the Lagrange identity

$$\psi_j L_j[\phi_j] - \phi_j L_j^\dagger[\psi_j] = \mathrm{d}/\mathrm{d}z\,[P_j(\phi, \psi)], \tag{41}$$

where $P_j(\phi, \psi)$ is the bilinear concomitant, defined by

$$\begin{aligned} P_j(\phi, \psi) = &-1/R_j[\psi_j(\phi_j''' - k_j^2\phi_j') - \phi_j(\psi_j''' - k_j^2\psi_j') + \phi_j'(\psi_j'' - k_j^2\psi_j) \\ &- \psi_j'(\phi_j'' - k_j^2\phi_j) + \mathrm{i}k_jR_j(\bar{u} - c_j)(\phi_j\psi_j' - \psi_j\phi_j') + \mathrm{i}k_jR_j\bar{u}'\phi_j\psi_j]. \end{aligned} \tag{42}$$

† These expressions are omitted for brevity. Copies may be obtained from the author or editorial office.

Integration across the range of the independent variable yields Green's formula

$$\int_0^\infty (\psi_j L_j[\phi_j] - \phi_j L_j^\dagger[\psi_j])\,\mathrm{d}z = [P_j(\phi,\psi)]_0^\infty. \tag{43}$$

Note that the range of integration is 0 to ∞. This is because we have eliminated the $O(\epsilon^2)$ wall displacement η_j from the second-order wall boundary conditions (38), writing the left-hand sides in terms of $\bar{\phi}_j$ only, and evaluating at the undisturbed wall position $z = 0$. In order to solve the linear flow equations numerically we of course have to impose outer boundary conditions at some finite value of z, but it is inappropriate to introduce these approximations at this stage (the formulation of the outer boundary conditions for numerical purposes will be discussed later).

We now rewrite the right-hand side of (43) as

$$[P_j(\phi,\psi)]_0^\infty = \sum_{i=1}^{8} U_i^{(j)} V_{9-i}^{(j)}, \tag{44}$$

where

$$\left.\begin{aligned} &U_1^{(j)} \equiv \phi_j'(0) + \frac{\bar{u}'(0)}{c_j}\phi_j(0), \quad U_2^{(j)} \equiv \phi_j'''(0) - 3k_j^2\phi_j'(0) - B_j\phi_j(0), \quad U_3^{(j)} \equiv \phi_j(\infty), \\ &U_4^{(j)} \equiv \phi_j'(\infty), \quad U_5^{(j)} \equiv \phi_j(0), \quad U_6^{(j)} \equiv \phi_j''(0) - (2k_j^2 - ik_jR_jc_j)\phi_j(0), \\ &U_7^{(j)} \equiv \phi_j''(\infty) - k_j^2\phi_j(\infty), \quad U_8^{(j)} \equiv \phi_j'''(\infty) - k_j^2\phi_j'(\infty) \end{aligned}\right\} \tag{45}$$

and

$$\left.\begin{aligned} &V_1^{(j)} \equiv -1/R_j\psi_j(\infty), \quad V_2^{(j)} \equiv 1/R_j\psi_j'(\infty), \quad V_3^{(j)} \equiv -1/R_j\psi_j'(0), \\ &V_4^{(j)} \equiv -\frac{1}{R_j}\left[\psi_j'''(0) + \frac{\bar{u}'(0)}{c_j}\psi_j''(0) + \left(\frac{k_j^2\,\bar{u}'(0)}{c_j} - B_j\right)\psi_j(0)\right], \\ &V_5^{(j)} \equiv -\frac{1}{R_j}[\psi_j''(\infty) - k_j^2\psi_j(\infty) - ik_jR_j(1-c_j)\psi_j(\infty)], \\ &V_6^{(j)} \equiv \frac{1}{R_j}[\psi_j'''(\infty) - k_j^2\psi_j'(\infty) - ik_jR_j(1-c_j)\phi_j'(\infty)], \\ &V_7^{(j)} \equiv \frac{1}{R_j}\psi_j(0), \quad V_8^{(j)} \equiv \frac{1}{R_j}[\psi_j''(0) + (k_j^2 + ik_jR_jc_j)\psi_j(0)]. \end{aligned}\right\} \tag{46}$$

The $O(\epsilon^2)$ boundary conditions for ϕ_j may now be re-expressed in terms of $U_1^{(j)}$, $U_2^{(j)}$, $U_3^{(j)}$ and $U_4^{(j)}$:

$$U_1^{(j)} = \mu_1^{(j)}, \quad U_2^{(j)} = \mu_2^{(j)}, \quad U_3^{(j)} = 0, \quad U_4^{(j)} = 0. \tag{47}$$

The general theory of differential systems (Ince 1956, §9.34) then attests that the boundary conditions for the homogeneous adjoint system must be

$$V_i^{(j)} = 0, \quad i = 1\text{–}4. \tag{48}$$

Furthermore, in order for the principal system given by (37), (38) and (39) to have a solution the following relation must obtain:

$$\int_0^\infty \psi_j r^{(j)}\,\mathrm{d}z = \mu_1^{(j)} V_8^{(j)} + \mu_2^{(j)} V_7^{(j)}. \tag{49}$$

After some rearrangement of (49), we arrive at the evolution equations

$$\sigma_3 \frac{\mathrm{d}A_3}{\mathrm{d}\tau} = \zeta_3 A_1 A_2, \quad \sigma_{1,2}\frac{\mathrm{d}A_{1,2}}{\mathrm{d}\tau} = \zeta_{1,2} A_{2,1}^* A_3. \tag{50a, b}$$

The quantities σ_j and ζ_j are lengthy and we do not give them here†. We define the quadratic interaction coefficients a_j by $a_j = \zeta_j/\sigma_j$, $j = 1, 2, 3$. For the rigid-wall case, the a_j have the form

$$a_3 = \frac{\int_0^\infty F_3 \psi_3 \, \mathrm{d}z}{A_1 A_2 \int_0^\infty \psi_3(\phi_3'' - \alpha^2 \phi_3) \, \mathrm{d}z}, \quad a_{1,2} = \frac{\int_0^\infty F_{1,2} \psi_{1,2} \, \mathrm{d}z}{A_3 A_{2,1}^* \int_0^\infty \psi_{1,2}(\phi_{1,2}'' - \gamma^2 \phi_{1,2}) \, \mathrm{d}z}, \tag{50c, d}$$

and are obtained as a special case: the reader is referred to Craik (1971) for the derivation of (50c, d).

4. Numerical method

An extension of the finite-difference method of Thomas (1953) was used for the boundary-layer computations presented below. This method utilizes a Noumerov auxiliary function to increase the accuracy of the differencing. The equations to be solved for the resonant-triad problem are: firstly the OS equation (23); then its adjoint, from (40); then the oblique OS equation for the 1-wave from (25), followed by its adjoint from (40); and finally the cross-flow equation for the 1-wave, from (26). For the linear, two-dimensional problem we only solve (23).

Approximations to the exact outer boundary conditions (17) and (36) are imposed at $z = z_1 \equiv 2.5\delta$, and 1000 grid points are used. The two physically relevant solutions of the OS equation are those which exhibit exponential decay at the respective rates $(-\alpha z)$ and $(-pz)$, where $p \equiv [\alpha^2 + \mathrm{i}\alpha R(1-c)]^{\frac{1}{2}}$, the root with positive real part being taken. The general solution at large z is then simply a linear combination of these two solutions so that

$$\phi \sim A\,\mathrm{e}^{-\alpha z} + B\,\mathrm{e}^{-pz},$$

where A, B are constants. The simplest differential operator which will annihilate the right-hand side above is $(\mathrm{D}+\alpha)(\mathrm{D}+p)$, $\mathrm{D} \equiv \mathrm{d}/\mathrm{d}z$, so the most appropriate *numerical* forms of the outer boundary conditions (3.7a, b) to be used at $z = z_1$, say, are

$$\phi'' + (\alpha+p)\phi' + \alpha p \phi = 0, \quad \phi''' + (\alpha+p)\phi'' + \alpha p \phi' = 0.$$

(These were suggested by Gill & Davey 1969). For the cross-flow velocity $\hat{v}_1$, we approximate (36) by $\hat{v}_1'(z_1) = [\gamma^2 + \mathrm{i}\gamma\tilde{R}(1-\tilde{c})]^{\frac{1}{2}} v_1(z_1)$, the root with negative real part being selected.

The program used by the author was developed from one supplied by Professor P. K. Sen. Eigenvalues are located by a combination of Newton–Raphson and *regula falsi* convergence schemes. The transverse wavenumber β for resonance is determined using the bisection method within the calculation of the eigenvalue $\tilde{c}$ subject to the condition that $\tilde{c}_\mathrm{r} = c_\mathrm{r}$. The iterative scheme in general requires a reasonably good initial estimate for the eigenvalue in order to converge, but this was often not available. Hence an alternative scheme based on the Principle of the Argument (PA) was developed, following Yeo (1986). A closed contour is traced out anticlockwise in the complex phase-speed plane, and the accumulated change in $\arg\{\det[A_{ij}]\}$ is $2n\pi$ if n eigenvalues are enclosed in the contour (assuming there are no singularities). If an eigenvalue is enclosed, the procedure is repeated continually using a reduced contour enclosing half the area of the original until at a prescribed limit the iteration

† Copies may be obtained from the author or editorial office.

procedure is invoked. This method is reliable, but costly in CPU time since the step length along the contour must be sufficiently small to avoid bypassing any loops. Hence the PA scheme was only used in the event of failure of the original initial-guess iteration routine.

Note that the OS equation and its adjoint have identical eigenvalue spectra: adjoint eigenfunctions were found by inserting the appropriate computed OS eigenvalue into the adjoint eigensystem. The error was then easily gauged from the magnitude of the bottom element of the upper-diagonal matrix which arises in the solution procedure. (This element is zero when the computed eigenvalue is exact.) Adjoint eigenvalues were also computed directly for a few cases, as an additional check.

The author has made a detailed comparison of his rigid-wall results with those of Hendriks (appendix to Usher & Craik 1975). Agreement is very good both for the linear data (that is, eigenvalues and eigenfunctions), and for the nonlinear data (that is, quadratic interaction coefficients), which confirms the soundness of both authors' numerical methods. More detail cannot be given because of space constraints.

Calculations were performed on a VAX 11/785 computer at the University of St. Andrews, and on Sun-4 workstations at the University of Exeter, using double precision arithmetic.

5. Linear results

5.1. *Walls without damping*

Eigenvalues for various values of α, R and the wall parameters $m^{(0)}$, c_0, $S^{(0)}$ have been calculated, and some of these are presented in figure 1. Here streamwise modes only are considered, and there is no wall damping ($d = 0$). As explained above, the quantities $m^{(0)}$ and $S^{(0)}$ are the values of mass per unit area and wall restoring force at a reference value R_0 of R (taken, arbitrarily, to be 2562.8 throughout). Three classes of wave mode were found, namely Tollmien–Schlichting (TS), wall flutter modes (which will be labelled F modes, and correspond to free waves on the flexible wall) and a class of slow-moving wall mode typically propagating upstream and having weak rates of amplification or damping (S modes). This latter class corresponds to the 'Kelvin–Helmholtz' (KH) mode class of Sen & Arora (1988). Examples of the three mode classes are shown in figure 1.

In the absence of modal interactions, TS mode eigenvalues are typically very similar to their rigid-wall counterparts, having c_r values between about 0.25 and 0.5 for the Reynolds numbers and wavenumbers considered herein. Since this work is principally concerned with resonant interactions, c_0 and S were mainly chosen to give wall modes having c_r similar to those for Tollmien–Schlichting (TS) modes. This was in order to allow the possibility of resonant triads formed from a mixture of mode types. Such values of c_0 and S have a tendency to produce strong linear interactions and ensuing very severe linear instability, as is shown by the $c_0 = 1.0$ case of figure 1, where $S = 0.15$. We can think of this as due to TS and F modes having opposite energy signs in an appropriate choice of reference frame. If modes of differing energy signs of two uncoupled systems are close to each other in some parameter space, then on coupling the systems they will interact and product linear instability (see for example Cairns 1979; Craik & Adam 1979). It should be noted, however, that there may be difficulties in applying these energy considerations to flows containing critical layers (see Craik 1985, §5).

For the F modes of figure 1, c_r decreases rapidly with wavenumber α. It is easy to

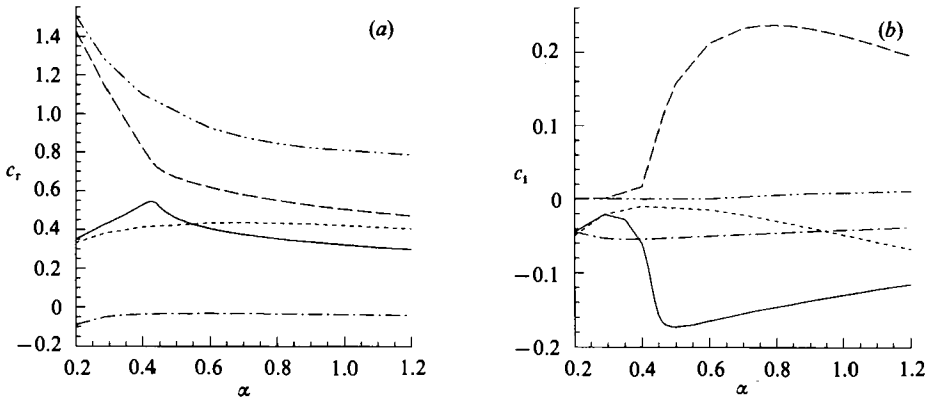

FIGURE 1. Linear dispersion curves: $m = 1.1$, $d = 0$, $S = 0.15$, $R = R_0 = 2562.8$. (*a*) c_r: —, TS, $c_0 = 0.1$; – – –, *F*, $c_0 = 0.1$; –·–, S, $c_0 = 0.1$; – – –, TS, $c_0 = 0.8$; –···–, F, $c_0 = 0.8$. (*b*) c_i: legend as in (*a*).

show that for the wall model (16) the behaviour of streamwise modes in the absence of wall damping is as follows:

$$c \sim \pm(c_0^2 + S/m\alpha^2)^{\frac{1}{2}}. \tag{51}$$

Thus for small values of c_0, as we have in figure 1, as α increases so c_r decreases as the inverse square of α; this is what is here observed. For the TS mode, c_r at first increases, but abruptly starts to decrease on reaching a certain closeness to the F-mode eigenvalue curve. After this point, the TS-mode curve mimics the F-mode curve. These two modes are in fact interacting, as is demonstrated by the curves for c_i. There is a huge 'bubble' of instability, the F mode being unstable and the TS mode stable, which commences at about the same value of α as the sudden change in the slope of c_r for the TS mode; the instability extends beyond the upper limit of the investigated wavenumbers α. The F and TS modes are analogous to the complex-conjugate pairs of the classical Kelvin–Helmholtz instability, with the important difference that the c_r values for the two modes remain distinct rather than coalescing. The non-coalescence of the modes is due to the dissipative influence of viscosity.

A stiffer wall ($c_0 = 0.8$ and $S = 0.15$) produces a general increase in c_r for the F mode whilst not affecting the corresponding TS value very much (figure 1). Thus the TS and F modes do not come as close to each other as for the previous case, and the c_r for the TS wave has no abrupt changes of slope. The interaction is weaker than for the less stiff wall, certainly for the range of wavenumbers considered: c_i for the F mode has a smaller maximum value. Another consequence of the weaker interaction is that the TS mode is less damped ($c_i \sim -0.05$ rather than -0.15).

The linear modal interactions behave rather like the modal coalescence of Carpenter & Garrad (1986), of Willis (1986), and of Thomas & Craik (1988), except that the values of c_r for the two interacting modes remain distinct rather than merging as is the case for true coalescence. The dispersion curves for c_i form upper and lower branches of a 'bubble', just like true coalescence, these typically being unstable and damped respectively (figure 1). The lack of proper coalescence may perhaps be due in part to the particular choices of parameter values used here (for example, the wall being relatively less or more flexible than those considered by Carpenter & Garrad and Willis, although it is not very meaningful to make such comparisons since the models are markedly different) or to the basic wall model itself, which is much simpler than that of the earlier authors. Willis considered the same wall model as Carpenter & Garrad, and found coalescence only with a viscous

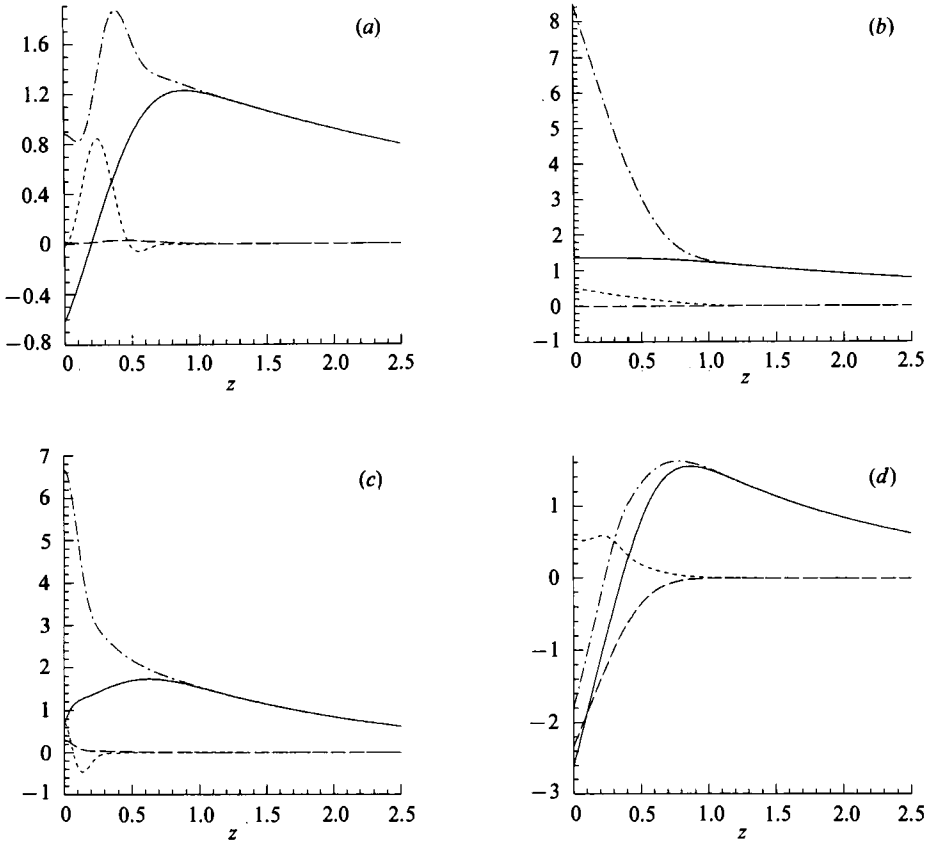

FIGURE 2. Eigenfunctions and adjoints: $m = 1.1$, $c_0 = 0.5$, $d = 0$, $S = 0.15$, $\alpha = 0.29056$, $R = R_0 = 2562.8$. (*a*) TS mode, $c = 0.4071 - 0.0198\mathrm{i}$: —, ϕ_r; – – –, ϕ_i; –·–, ψ_r; ---, ψ_i. (*b*) F mode, $c = 1.1914 + 0.0009\mathrm{i}$: legend as (*a*). (*c*) $\alpha = 0.6$, S mode, $c = -0.1122 - 0.0413\mathrm{i}$: legend as (*a*). (*d*) $\alpha = 0.6$:—, F mode, $c = 0.6846 + 0.0856$, ϕ_r; – – –, ϕ_i; –·–, TS mode, $c = 0.4776 - 0.1166\mathrm{i}$, ϕ_r; ---, ϕ_i.

substrate present. He conjectured that it also occurs in the presence of an inviscid substrate, but only for *complex* values of wavenumber and frequency, and is consequently much harder to observe in this case.

The eigenfunctions of the TS, F and S classes have distinctive shapes, as can be seen from figure 2. Here and elsewhere all eigenfunctions ϕ and adjoints ψ are normalized to unity at $z = 1.7208$, that is at five displacement thicknesses from the wall; this normalization was used by Hendriks (appendix to Usher & Craik 1975). The eigenfunction for the Tollmien–Schlichting wave is depicted in figure 2(*a*), and is very similar to a typical rigid wall TS eigenmode. This is also true of the adjoint eigenfunction.

The F-mode eigenfunction is completely different in shape to that of the TS mode, as can be seen from figure 2(*b*). The normal velocity (of which ϕ is a measure) has its maximum at the wall and decreases rapidly with increasing z. This is of course expected for wall modes. The large value of ϕ_w (that is, ϕ evaluated at the wall) is a consequence of normalization being imposed in the free stream rather than at the wall. The F-mode adjoint eigenfunction also has a characteristic shape (figure 2b), with an extremely small imaginary part.

The S-class mode eigenfunction, illustrated in figure 2(*c*), has a real part which

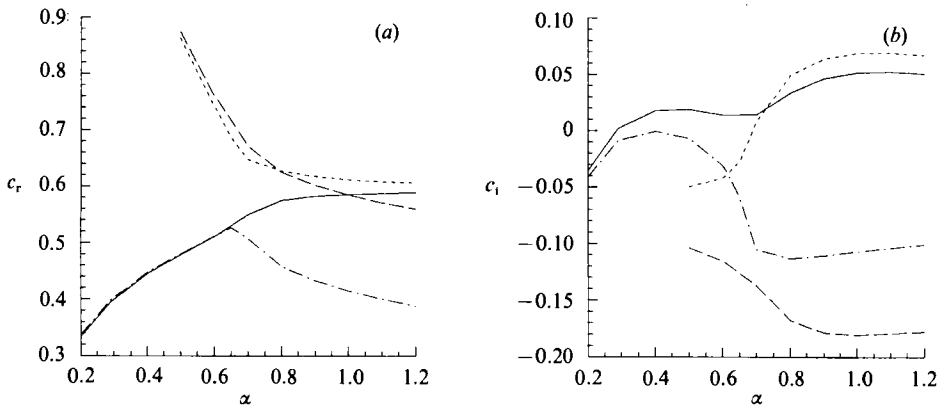

FIGURE 3. Linear dispersion curves: $m = 1.1$, $c_0 = 0.6$, $S = 0.15$, $R = R_0 = 2562.8$. (*a*) c_r: —, TS, $d = 0.05$; – – –, F, $d = 0.05$; –·–, TS, $d = 0.1$; ---, F, $d = 0.1$. (*b*) c_i: legend as in (*a*).

bears some resemblance to ϕ_r for TS modes, although there is a 'kink' near the wall. The shape of the S-class eigenfunction is in fact just like that of the KH-mode-class eigenfunction given in Sen & Arora (1988), and we may therefore state with confidence that these classes are equivalent. Note that the S-mode adjoint eigenfunction (figure 2*c*) bears no resemblance to that for the TS mode.

Figure 2(*d*) depicts an F mode and a TS mode at a wavenumber of $\alpha = 0.6$, larger than that for figures 2(*a*) and 2(*b*). Here the TS and F modes are interacting linearly. The most remarkable feature is that ϕ_r for the F mode has changed drastically in shape from that of figure 2(*b*), and now is virtually indistinguishable from a TS mode. The imaginary part ϕ_i has retained its profile, albeit reflected about the z-axis and considerably increased in magnitude. Comparison of figures 2(*d*) and 2(*a*) reveals much less dramatic changes for the TS mode – the main one being an increase in the size of ϕ_i. The character of the F-mode eigenfunction is dependent upon whether c_r is greater or smaller than unity: if $c_r > 1$, then there is no critical layer. Note that F modes can be linearly unstable even for $c_r > 1$; this is in agreement with the findings of Sen & Arora (1988) and Carpenter & Gajjar (1990).

5.2. *Walls with damping*

Introduction of linear damping d to the wall model can have a significant effect on these modal interactions, as we shall now see. In figure 3 c_0 has a value of 0.6; the restoring-force parameter $S = 0.15$ is however the same as for the examples in figure 1. Thus the instability due to modal interaction has a strength intermediate to those earlier examples. The plots of c_r and c_i for the TS and F modes for the $D = 0.05$ case of figure 3 are similar to those in figure 1, except that the TS mode is now less damped than the F mode for wavenumbers α less than about 0.6. The F mode again forms the upper branch of the 'bubble', which is however displaced to wavenumbers a little higher than that shown in figure 1. The maximum value of c_i for the F mode is about 0.08, indicating a moderately strong instability.

A larger damping factor $d = 0.1$ radically alters the characteristics of the dispersion curves (figure 3). The c_r curves for the TS and F modes now cross one another, at $\alpha \approx 1.0$, and the region of instability extends to smaller wavenumbers. It is now the TS mode which is unstable: it has exchanged roles with the F mode, which is now damped. This reversal of the modal stability characteristics is due to the fundamentally different effects of damping on the TS and F modes: the former are Class A and hence destabilized by damping, whilst the latter being Class B are

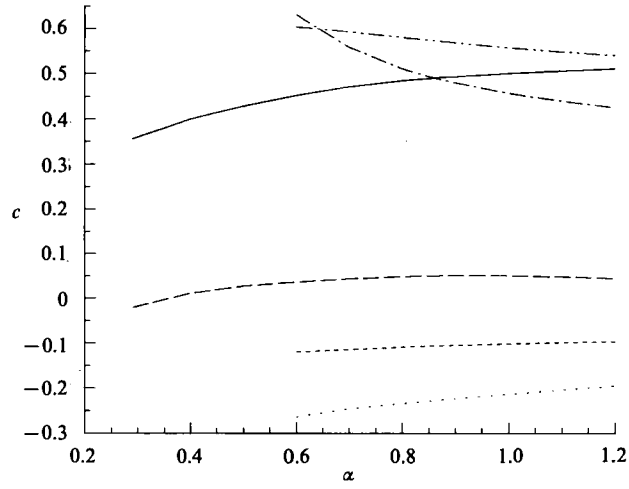

FIGURE 4. Linear curves: $m = 2$, $c_0 = 0.5$, $d = 0.2$, $S = 0.3$, $R = 2000$, $R_0 = 2562.8$. —, c_r(TS); – – –, c_i(TS); –·–, c_r(F); – – –, c_i(F); –··–, c_r(HO); ····, c_i (HO).

stabilized. These energy classes were postulated by Benjamin (1963) and Landahl (1962). Note that the maximum value of c_i (for the range of wavenumbers considered) is reduced from ~ 0.07 to ~ 0.05 by the increase in damping; but this beneficial effect must be weighed against the increase in the range of wavenumbers for which there are unstable eigenmodes.

The S-mode-class waves are rendered less stable by wall damping, suggesting that they are Class A, (and hence perhaps upstream-propagating TS waves). There has been very little work done on upstream-propagating TS waves for any OS problem, other than the derivation of formal bounds for the eigenvalues (Joseph 1968, 1969), although Mack (1984) does briefly mention them in the context of the spatial stability problem. However, the eigenvalues for these waves are more sensitive to changes in the wall parameters than is expected for fluid modes, to such an extent that the author was unable to keep track of them or to find rigid-wall analogues. This suggests that they are in fact upstream-propagating wall modes. Sen & Arora (1988) clearly take the latter view, since they regard their KH modes as 'stationary periodic ripples' in the limit of $|c| \to 0$. Examination of the *adjoint* eigenfunction (figure 2*c*) also leads to the conclusion that the S mode is wall-based.

5.3. *Other fluid modes*

In addition to the three mode types already described, there also exist higher-order fluid modes (see for example Mack 1976, where these are discussed for the rigid-wall configuration) and oblique Squire modes of $\hat{v}$. The former category falls into two distinct groups, comprising discrete and continuous parts of the eigenvalue spectrum. These are in general heavily damped and hence often considered to be of little practical interest, although as α or R increases they migrate towards $c = 0$ in the (complex) phase-speed plane (that is, they become less damped). It has been suggested that the continuous spectrum plays a role in the transfer of energy between the boundary layer and the free stream (Corner, Houston & Ross 1976), because the associated perturbation velocities can remain significant at the edge of the boundary layer and beyond. An example of a higher-order (HO) mode belonging to the discrete part of the spectrum is depicted in figure 4, where a damping level $d = 0.2$ applies. The HO eigenfunction and adjoint and those of the F mode are shown in figures

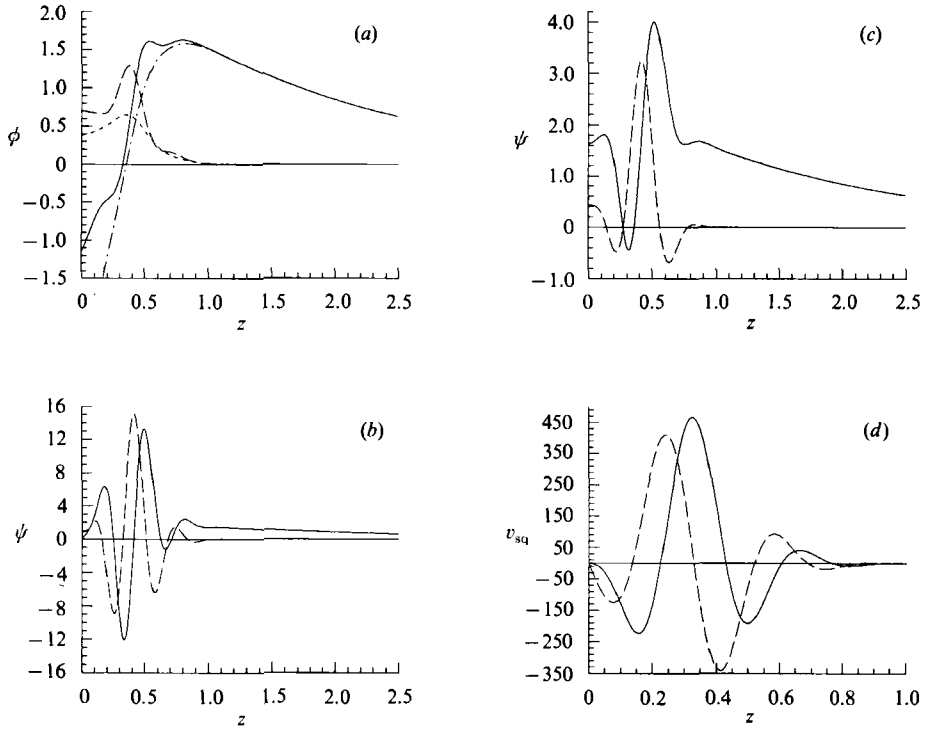

FIGURE 5. $\alpha = 0.6$: other parameters as figure 4. (*a*) —, HO mode, ϕ_r; ---, HO mode, ϕ_i; -·-, F mode, ϕ_r (cuts vertical axis at -2.829); ···, F mode, ϕ_i. (*b*) HO mode: —, ψ_r; ---, ψ_i. (*c*) F mode: —, ψ_r; ---, ψ_i. (*d*) Squire mode velocity v_{sq}. $\alpha = 1.0, \beta = 1.1041, c = 0.5008 - 0.2806\mathrm{i}$: —, v_{sqr}; ---, v_{sqi}.

5(*a*)–5(*c*), for a wavenumber of 0.6. The TS and F eigenmodes (real parts) cross at $\alpha \approx 0.86$, as do the F and HO eigenmodes at $\alpha \approx 0.65$, just larger than the value at which we have sample plots of the eigenfunctions. The TS mode is unstable, with c_i having a maximum value of ~ 0.05. The F mode is strongly damped owing to the presence of wall damping, with $c_i \approx -0.1$; and the HO is rather more heavily damped, having $c_i \approx -0.2$. The F mode strongly resembles a typical TS mode, as was the case in figure 2(*d*). The HO mode also has some similarity with TS modes, but there are distinctive 'wobbles' in the profile of ϕ_r. The peaks in ϕ_i for the two modes are located at the critical point, where $c_r = \bar{u}$. Examination of the adjoints reveals remarkable similarities between them (and considerable differences from any previously considered). It seems that these modes are interacting in some way, although there is no evidence of this in the behaviour of c_i for these modes in figure 4. We are in no doubt that the F mode has been correctly identified – the dispersion curves for $d = 0$ (no wall damping) are qualitatively very similar, in both real and imaginary parts, to those cases already considered in figure 1, though we do not present them herein.

Squire modes are solutions to the homogeneous version of (26), that is

$$\hat{v}_{sq}'' - [\gamma^2 + \mathrm{i}\gamma\tilde{R}(\bar{u} - c_{sq})]\,\hat{v}_{sq} = 0. \tag{52}$$

The outer boundary condition is the same as for the cross-flow velocities $\hat{v}_{1,2}$, that is (36), but at the wall we have the simple condition $\hat{v}_{sq}(0) = 0$. This is because Squire

modes have no vertical velocity component, and hence cannot induce any displacement of the wall from its undisturbed position. Thus *in the linear limit* there is no difference between Squire modes over flexible walls and their rigid-wall counterparts, at the same values of α and R. The 'Squire equation' (52) is an eigensystem in its own right, with a spectrum of eigenvalues c_{sq}. It is known that these are all damped (see Davey & Reid 1977, where the mathematically equivalent problem of temperature modes in a stratified fluid is studied; and also Murdock & Stewartson 1977, where the plane Poiseuille problem is investigated via a model equation). However, they may resonate linearly or nonlinearly with the eigenvalues of the OS system, either exactly or approximately, and therefore should not be overlooked.

Solutions to the Squire-mode equation are somewhat similar to the two viscous solutions of the OS equation. There is a continuous spectrum of damped modes with $c_r = 1$, together with a set of discrete modes having smaller c_r. Interactions between TS and Squire modes in boundary-layer flow have been examined for the case of spatial disturbances by Nayfeh (1985): he found that the interactions could be strong, implying that they represent an additional means of amplifying three-dimensional effects. Linear resonance between OS and Squire modes has been studied by Gustavsson & Hultgren (1980) for plane Couette flow, by Gustavsson (1981) for plane Poiseuille flow, and by Hultgren & Gustavsson (1981) for boundary-layer flow. Herbert (1983, 1988) has studied forms of nonlinear instability in rigid-wall flows (that is, three-dimensional effects that follow the Tollmien–Schlichting instability); he found that near-resonant triads can be formed between a TS wave and a pair of (highly damped) Squire modes.

A few Squire modes were located using the PA scheme referred to above: these are displayed in table 3 below, and a typical eigenfunction is pictured in figure 5(*d*). Note that the outer limit of integration is δ, not 2.5δ; convergence was severely impaired at the larger value.

6. Nonlinear results

6.1. *Triads of TS waves*

Resonant triads of the Craik form, comprising three TS waves, were located mainly for one set of wall parameters, but considering a side range of wavenumbers α and Reynolds numbers R, and are presented in figures 6–8, together with rigid-wall counterparts.

It will be seen from figures 6–8 that the quadratic interaction coefficient a_3 for the streamwise modes always remains $O(1)$ in magnitude, in marked contrast to its oblique counterpart a_1, the modulus of which increases very substantially with both wavenumber and Reynolds number. These results have similarities with those of Volodin & Zel'man (1979) for spatial wave modes. It would appear from the $a = 1.0$ cases (figure 8) that a_1 may decrease for sufficiently large R, although the evidence is only provided by a single data point. Note that by symmetry $a_2 = a_1$, and the a_j are all *complex*.

The spanwise wavenumber β of the oblique constituents of the triads generally increases with increasing α but decreases with increasing R. The propagation angle θ of these waves decreases with both wavenumber and Reynolds number, as will be shown later.

Comparison of the present results with those of Smith & Stewart's (1987) asymptotic analysis is not straightforward. This is because the latter authors assume

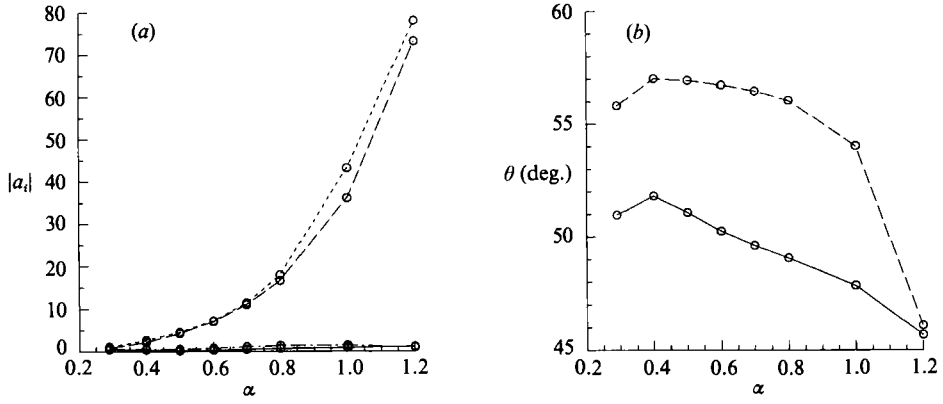

FIGURE 6. (*a*) Quadratic interaction coefficients $|a_1|$, $|a_3|$ versus streamwise wavenumber α: $m = 2$, $c_0 = 0.5$, $d = 0$, $S = 1$, $R = R_0 = 2562.8$. Triads comprise three TS modes. —, $|a_1|$ (rigid); – – –, $|a_1|$ (compliant); –·–, $|a_3|$ (rigid); ---, $|a_3|$ (compliant). (*b*) Oblique-wave propagation angle θ (degrees): parameters as in (*a*). —, rigid; – – –, compliant.

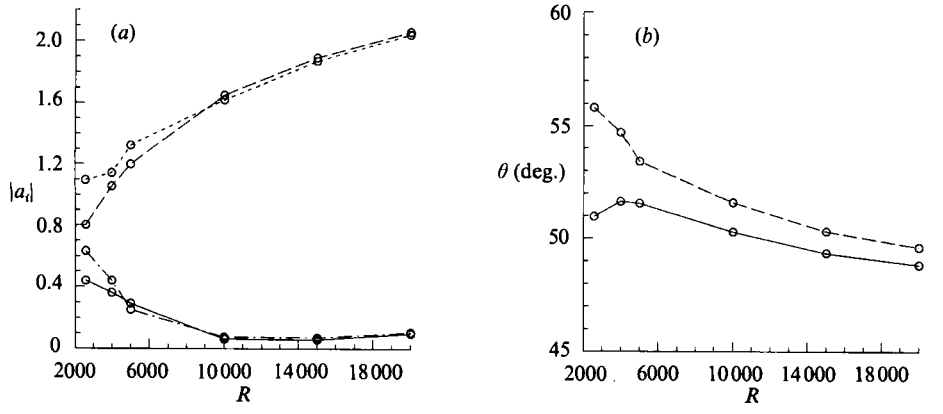

FIGURE 7. (*a*) Quadratic interaction coefficients $|a_1|$, $|a_3|$ versus Reynolds number R: $\alpha = 0.29056$, $R_0 = 2562.8$; wall parameters as figure 6. Triads comprise three TS modes. —, $|a_1|$ (rigid); – – –, $|a_1|$ (compliant); –·–, $|a_3|$ (rigid); ---, $|a_3|$ (compliant). (*b*) Oblique-wave propagation angle θ (degrees): parameters as in (*a*). —, rigid; – – –, compliant.

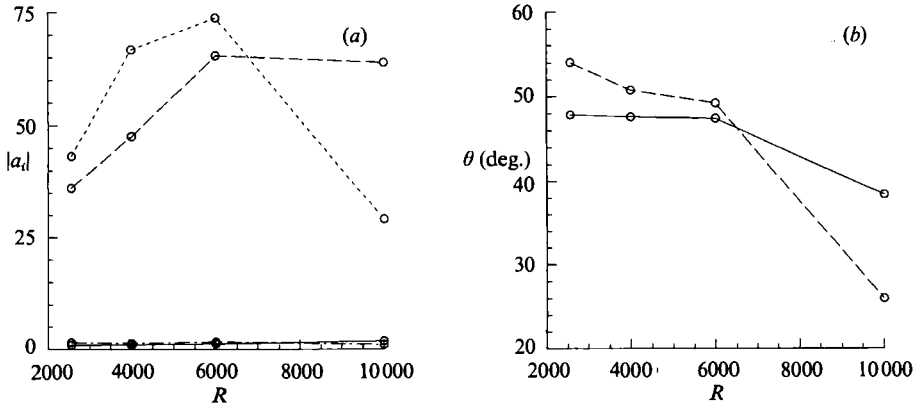

FIGURE 8. As figure 7, except $\alpha = 1.0$.

that the resonating wave modes, having frequencies ω that are large but less than $O(R^{\frac{1}{4}})$ as $R \to \infty$, lie asymptotically close to the lower-branch neutral curve, conditions which are certainly not satisfied by the triads of figures 6–8.

The interaction coefficients a_1, a_3 which are presented in figures 6–8 are complex, not real, quantities and so it follows that finite-time blow-up of the (truncated) equations (50) is possible, this being an important difference from the scenario studied by Smith & Stewart. Also, the propagation angles $\theta = \cos^{-1}(\alpha/2\gamma)$ for the oblique-mode triad constituents are never very close to the inviscid, high-frequency value of 60° obtained by asymptotic analysis: they are always less than this, and indeed decrease with increasing α or R. The wall parameters were selected to emulate a wall that is stiff enough to preclude linear modal interactions. The real part of phase speed, c_r, is generally higher than for the equivalent rigid-wall case. It is difficult to make any firm observations on the effect of surface compliance on linear stability from these results, except to say that in the main both the streamwise and oblique modes are a little more amplified (or less damped) than their rigid-wall analogues; this indicates that the wall parameters selected here are not beneficial in promoting transition delay.

Quadratic interaction coefficient moduli are plotted against wavenumber at constant R in figure 6(a), along with the corresponding rigid-wall values. It will be seen that the difference between the two cases in terms of these coefficients is only small, although the compliant-wall values are usually larger. A comparison of the propagation angles θ of the oblique constituents of the triads for the two configurations (figure 6b) reveals that the obliquity is consistently greater for compliant wall flow than for rigid wall flow. Quadratic interaction coefficient moduli and propagation angles are plotted against Reynolds number for (fixed) $\alpha = 0.29056$ in figure 7, and for $\alpha = 1.0$ in figure 8. Here differences between the rigid and compliant cases are a little more apparent, although they remain broadly similar. For $\alpha = 1.0$, the oblique coefficients at first increase in magnitude with R, but eventually begin to decrease. The propagation angles θ decrease with R as they do with α, but more markedly.

A few results have also been obtained for a slightly stiffer wall ($S^{(0)} = 2$): they cannot be presented fully because of lack of space. Once again, there is no consistent trend in the linear stability data, although c_i is smaller than for the less stiff wall and larger than for the rigid wall (which is as expected, since the rigid wall corresponds to the limit of infinite stiffness). The quadratic interaction coefficients are however always a little smaller in magnitude than for the less stiff wall; this indicates that wall flexibility has a reinforcing effect on the strength of resonant triad interactions, even though no wall modes are participating.

6.2. *Mixed-mode triads without wall damping*

It was envisaged at the outset that resonant triads comprising a mixture of TS and other modes would be of particular interest. However, as has already been mentioned, location of such triads was hampered by the presence of modal coalescence or near-coalescence. Indeed, the author was unable to locate any mixed-mode triads that were free from linear modal interaction.

It is quite difficult to locate any triads with oblique wall (F) mode constituents: this is because the eigenvalue $\tilde{c}$ for such modes (the free-wave speed on the wall) varies with α according to

$$\tilde{c}_r \sim \pm\left(\frac{\alpha}{2\gamma}c_0^2 + \frac{4S}{m\alpha^2}\right)^{\frac{1}{2}}, \tag{53}$$

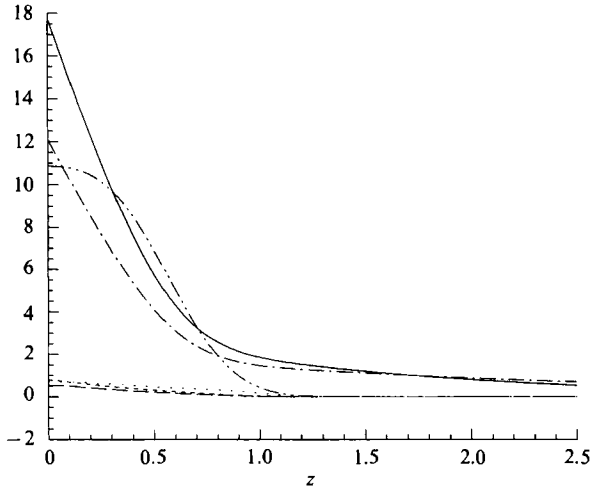

FIGURE 9. Triad comprising three wall modes: $\alpha = 0.8$, $R = R_0 = 2562.8$, $m = 2$, $c_0 = 1.2$, $d = 0$, $S = 0.1$. —, ϕ_{3r}; ——, ϕ_{3i}; –·–, ϕ_{1r}; – – –, ϕ_{1i}; –·–·–, $\hat{v}_{1r}$; ····, $\hat{v}_{1i}$.

	α	β	$\tilde{R}$	c_r	c_i	$\tilde{c}_i$	$\lvert a_3\rvert$	$\lvert a_1\rvert$
(*a*)	0.8	0.3310	1974.4	0.3824	0.0039	−0.0068	0.31	15.55
	0.8	0.2508	2171.3	1.1577	−0.0002	0.0001	2.39	89.48
(*b*)	1.2	0.8729	1451.7	0.7872	0.111	0.0128	1.39	130.45
(*c*)	1.0	0.5317	10276.0	0.3525	−0.0390	−0.1125	0.60	6373.0
	1.0	0.8101	7878.4	0.3635	−0.0418	−0.0904	4.22	8544.0

TABLE 1. Compliant wall, resonant triads. $R_0 = 2562.8$. (*a*) $R = 2562.8$, $m^{(0)} = 2.0$, $c_0 = 1.2$, $d = 0$, $S^{(0)} = 0.1$: first row is a triad of three TS modes, second row is a triad of three F modes (figure 9); (*b*) $R = 2562.8$, $m^{(0)} = 1.1$, $c_0 = 0.8$, $d = 0$, $S^{(0)} = 0.15$: triad of three F modes; (*c*) $R = 15000$, first row is rigid wall, for second row $m^{(0)} = 2.0$, $c_0 = 0.5$, $d = 0$, $S^{(0)} = 1.0$: in both cases triad comprises a streamwise TS mode and two oblique HO modes.

in the absence of wall damping. Note the differences between (53) and (51): the factor $\alpha/2\gamma$ is due to the particular form of tension we have selected; but the extra 4 in the restoring-force term arises from the periodicity $\exp\{\mathrm{i}(\frac{1}{2}\alpha x \pm \beta y - \frac{1}{2}\alpha\tilde{c}t)\}$ that is required for Craik-type resonance. The effect is generally to make $\tilde{c}$ much larger than c, which obviously is detrimental to the location of resonant triads.

Triads comprising three wall modes have nevertheless been located, and two examples are given in table 1. The oblique interaction coefficients $|a_1|$ are large, being $O(100)$ whilst the streamwise coefficient $|a_3|$ remains $O(1)$. (Note that in each case there is some linear instability, and for the second wall-mode triad presented c_i and $\tilde{c}_i$ are both rather large at $O(10^{-2}.)$ A TS-mode triad at the same values of α, R and wall parameters as one of the wall triads is also given, and it will be observed that a_1 for the TS triad is substantially less than for the wall-mode triad (note also the comparative smallness of the propagation angles θ for the oblique modes in both cases). The eigenfunctions, their adjoints and the cross-flow velocity are presented in figure 9.

Triads formed of a streamwise TS wave and a pair of oblique HO modes have been located at a Reynolds number of 15000, and are presented in table 1 for both rigid-wall and compliant-wall configurations. The oblique modes are significantly damped

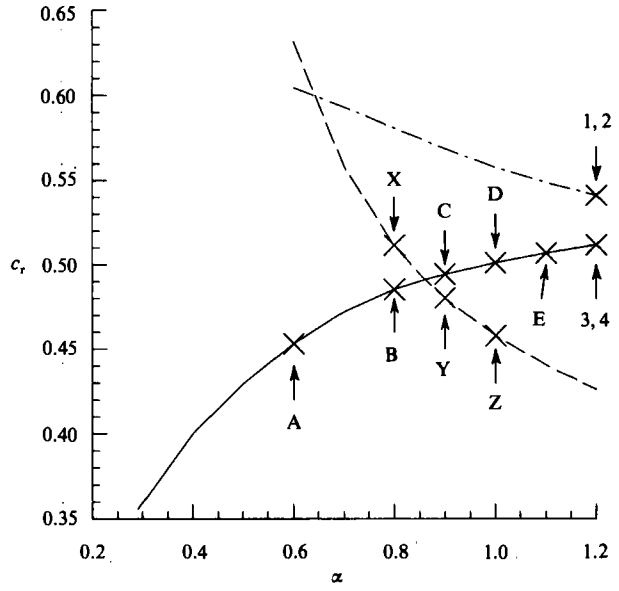

FIGURE 10. As figure 4; marked points are the locations of streamwise constituents of resonant triads (see also figure 12, table 2).

in the linear regime ($c_i \approx 0.1$) but nevertheless have remarkably large oblique quadratic interaction coefficients a_1, these being $O(8000)$ in modulus for the compliant wall and $O(6000)$ for the rigid wall; the a_3 remain $O(1)$ in magnitude. These particular triads could be deemed of no practical significance because of their rather strong linear damping, but examples exhibiting less severe damping may well be possible.

6.3. *Mixed-mode triads with wall damping*

The presence of linear modal interaction has a strong influence on the nature of resonant triad interactions. Figure 10 shows dispersion curves for three modes, namely a TS, an F and an HO fluid mode. A damping coefficient $d = 0.2$ applies here. The TS- and F-mode phase speeds (real parts) cross at $\alpha \approx 0.86$, and a significant linear interaction is indicated by the relatively large magnitude of c_i for both these modes (see figure 4). This particular scenario admits a wide variety of resonant triad configurations, involving all three of the different mode types here present. Triads have been located at the various points marked on the curves. Points A, B, C, D, E indicate the eigenvalues of streamwise constituents of resonant triads, where all three participating modes are of TS type. In each case the streamwise mode is undergoing a linear interaction with the streamwise F mode (the interaction occurs over a wide range of wavenumbers α, as can be inferred from figure 4). It is the TS mode which is driven unstable ($c_i \approx 0.05$ at most), but the wall damping mitigates the severity of the instability (if $d = 0$ rather than 0.2, then $c_i \approx 0.088$ at most for the F mode). Points X, Y, Z correspond to a streamwise wall mode interacting resonantly with a pair of oblique TS modes. Some of the triads located are tabulated in table 2. The various points A–E, X–Z just represent particular examples of the triads that may be constructed: there are in fact two continua of points representing triads, each of which extends some distance along the TS- and F-mode dispersion curves.

The quadratic interaction coefficients for the heterogeneous TS triads are highly interesting as can be seen from figure 11: $|a_1|$ has a sharp spike centred at about

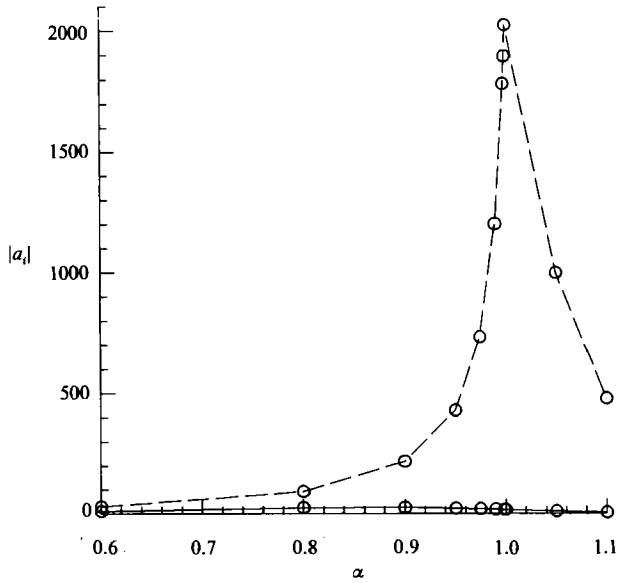

FIGURE 11. Quadratic interaction coefficients $|a_1|$, $|a_3|$ versus wavenumber α: parameters as figure 4. Triads comprise three TS modes. —, $|a_3|$; – – –, $|a_1|$.

		α	β	$\tilde{R}$	c_r	c_i	$\tilde{c}_i$	$\lvert a_3\rvert$	$\lvert a_1\rvert$
(*a*)	X	0.8	1.4693	525.4	0.5115	−0.1087	−0.0482	72.32	50.63
	Y	0.9	0.9286	872.2	0.4803	−0.1046	−0.0203	4.00	85.15
	Z	1.0	0.4571	1476.1	0.4579	−0.1012	−0.0015	0.40	76.1
(*b*)	1	1.2	0.5698	1450.3	0.5412	−0.1951	−0.0576	2.59	205.1
	2	1.2	1.0075	1023.4	0.5412	−0.1951	0.0112	7.23	107.9
	3	1.2	0.5704	1449.6	0.5117	0.0446	0.0011	0.41	338.1
	4	1.2	0.8752	1130.9	0.5117	0.0446	−0.0754	4.87	266.1

TABLE 2. Compliant wall, resonant triads (figure 10). $R_0 = 2562.8$, $R = 2000$, $m^{(0)} = 2.0$, $c_0 = 0.5$, $d = 0.2$, $S^{(0)} = 0.3$: (*a*) triads formed of one streamwise wall wave and two oblique TS waves; (*b*) case 1: HO wave and two oblique wall waves; case 2: HO wave and two oblique TS waves; case 3: three TS waves; case 4: TS wave and two oblique wall waves.

$\alpha = 1.0$, with maximum magnitude of approximately 2000. The streamwise coefficient a_3 behaves much less spectacularly, being $O(10)$ in magnitude and having its maximum in the region $\alpha = 0.8$–0.9. Note however that $|a_3|$ is an order of magnitude larger than has hitherto been normal for TS triads. The propagation angles θ are somewhat larger than previously, decreasing with α from $\sim 69°$ to about $57°$.

The triad located at $\alpha = 1.0$ (near the tip of the spike in $|a_1|$) has cross-flow velocity and derivatives which are large in magnitude relative to other triads, and it is these functions which give rise to the unusually large value of $|a_1|$. It is probable that the large values of $\hat{v}$ are due to linear interaction between an oblique TS mode and a Squire mode at $\alpha \approx 1.0$, $\beta \approx 1.104$, $\tilde{c}_r \approx c_{sqr} \approx 0.5010$ (table 3). (This is not a true linear resonance, such as was studied by Gustavsson & Hultgren (1980), since $\tilde{a}_i$ and c_{sqi} are not close to each other).

The interactions at points X, Y, Z are also interesting (table 2, figure 10): at point X, the streamwise triad component experiences a *stronger* resonant interaction than

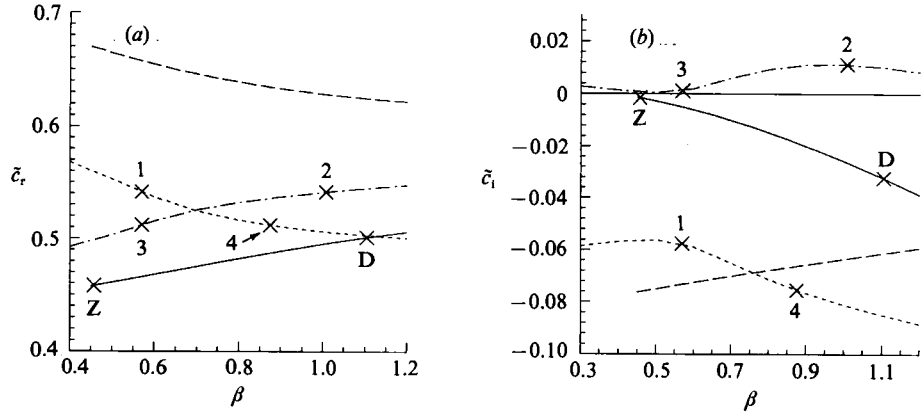

FIGURE 12. Variation of eigenvalue $\tilde{c}$ of oblique waves with transverse wavenumber β, showing effect of change in streamwise wavenumber α: parameters as figure 4. Marked points are the locations of oblique constituents of resonant triads (see also figure 10, table 2). (*a*) $\tilde{c}_r$: —, TS, $\alpha = 1.0$; – – –, F, $\alpha = 1.0$; –·–, TS, $\alpha = 1.2$; ---, F, $\alpha = 1.2$. (*b*) $\tilde{c}_i$; legend as in (*a*).

α	β	c_r	c_i	$\tilde{c}_i$	$\lvert a_3\rvert$	$\lvert a_1\rvert$	c_{sqr}	c_{sqi}	ϵ
0.95	1.1407	0.4980	0.0509	−0.0323	21.98	429.5	0.5097	−0.2852	0.0117
0.99	1.1154	0.5006	0.0506	−0.0325	17.70	1201	0.5026	−0.2815	0.0020
0.998	1.1066	0.5011	0.0505	−0.0323	16.69	1783	0.5012	−0.2808	0.0001
0.999	1.1053	0.5011	0.0505	−0.0323	16.58	1895	0.5010	−0.2807	−0.0001
1.0	1.1041	0.5012	0.0504	−0.0323	16.4	2020	0.5008	−0.2806	−0.0004
1.0	1.1041	—	—	—	—	—	0.2845	−0.1644	—
1.1	0.8582	0.5068	0.0481	−0.0208	4.18	477.8	0.4848	−0.2720	−0.0220

TABLE 3. Orr–Sommerfeld resonant triads and Squire equation eigenvalues. Wall parameters as in table 2. We define $\epsilon \equiv c_{sqr} - \tilde{c}_r$. See also figure 11.

its oblique counterparts ($|a_3| > |a_1|$), though as α increases this interaction weakens rapidly unlike the oblique ones. The oblique-wave propagation angle θ also changes substantially as α increases from 0.8 to 1.0.

Points 1–4 of figure 10 and table 2 designate the linear eigenvalues of the streamwise constituents of four different resonant triads that have been located for a streamwise wavenumber $\alpha = 1.2$. For points 1 and 2 the streamwise mode is a higher-order fluid mode, whereas for points 3 and 4 the streamwise mode is a TS mode. The two oblique constituents of these four triads are of the following mode-classes: for point 1, wall (F); for point 2, TS; for point 3, TS; for point 4, wall (F). For each of the triads the oblique modes experience strong resonant interaction, as indicated by the values of $|a_1|$, which are all $O(100)$. The triad at point 3, comprising three TS waves, has the largest value of $|a_1|$, but by contrast also has the smallest value of the streamwise coefficient $|a_3|$.

Dispersion curves of $\tilde{c}$ versus the transverse wavenumber β, at fixed values 1.0 and 1.2 of α are given in figure 12. Both oblique TS- and oblique F-mode eigenvalues are shown, plus the locations of computed resonant triads. A linear interaction is taking place between the TS and F modes, which increases with increasing α. The mode-crossing phenomenon that is a feature of linear interactions in the presence of wall damping is observed to occur at $\alpha = 1.2$, but not at the smaller value of α. Eigenfunctions and cross-flow velocity for the triad at point 1 are given in figure 13.

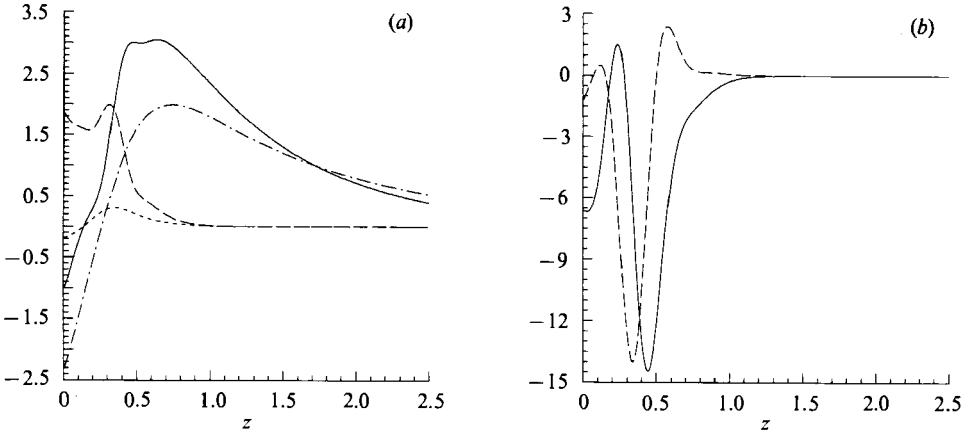

FIGURE 13. Resonant triad at point 1 of figure 10. (*a*) Eigenfunctions: —, ϕ_{3r}; – – –, ϕ_{3i}; –·–, ϕ_{1r}; ---, ϕ_{1i}. (*b*) Cross-flow velocity: —, $\hat{v}_{1r}$; – – –, $\hat{v}_{1i}$.

In figure 13, we see that ϕ_3 has the distinctive profile of higher-order fluid modes; and ϕ_{3i} has a strong peak, which is in fact located at the critical point z_c. The oblique F-mode ϕ_1 looks like a TS mode, but the maximum value is in fact at the wall. The cross-flow velocity $\hat{v}_1$ is very much like that for a typical rigid-wall TS-mode triad (Usher & Craik 1975).

When considering the relative magnitudes of quadratic interaction coefficients a_3, a_1 for different resonant triads, and even within the same triad, it must be remembered that these magnitudes are dependent on the normalizations employed for ϕ_j and ψ_j. This is particularly important when comparing wall modes (F or S) with fluid modes (TS or HO). The obvious normalization to employ for wall modes is to set ϕ_w equal to some constant, say unity, but that is not very suitable for fluid modes, especially when one is also considering the rigid-wall problem. We have imposed normalization at a point away from the wall because this permits investigation of both scenarios.

7. Conclusions

7.1. *The linear regime*

We have found and examined five distinct classes of wave mode for the problem of Blasius flow over flexible walls, which we labelled TS, HO, F, S and Squire modes. The Tollmein–Schlichting (TS) class has very similar properties to its rigid-wall counterpart, as does the HO class of discrete higher-order wave modes. The class of wall modes which we have termed F modes is identifiable with the TWF of Carpenter & Garrad (1986), and the CIFI of Yeo (1986); the S class corresponds to the KH class of Sen & Arora (1988), and to the divergence class of Carpenter & Morris (1990).

The stability of TS modes is determined in the absence of modal interaction principally by the values of wavenumber α and Reynolds number R, being much less dependent on wall parameter values. The F modes, being fundamentally inviscid in character, are typically very close to a state of neutral stability, again provided they are not participating in modal interaction. The S modes that have been located for various walls have a tendency to be very slow moving ($c_i \approx 0$), usually in the upstream direction, and have small to moderate ($-0.05 < c_i < 0$) rates of linear damping. We

believe these to be wall modes, although this has not been definitely established. The HO modes tend not to be especially interesting, at least in the linear regime, as they are strongly damped except for very large values of α and/or R.

Linear modal interaction between TS waves (Class A) and F waves (Class B) almost invariably produces strong instability of one or other of the participating modes. Such interactions have some similarity to the classical Kelvin–Helmholtz instability – the c_i versus α curves for the two modes have the familiar 'bubble' shape, the extent of this bubble indicating the range of wavenumbers over which linear interaction is occurring. There are important differences, however: the c_r values of the modes do not coincide during the interaction but remain distinct, that is there is no *coalescence*; and the phenomena of quasi-Kelvin–Helmholtz instability and modal exchange of identities are not mutually exclusive, unlike non-dissipative cases such as that studied in Thomas & Craik (1988).

Clearly such instabilities are most undesirable if the aim is to delay transition, and they are best avoided by choosing walls which have sufficient stiffness to render c_r for the F modes appreciably larger than c_r for TS modes at all relevant values of α and R.

7.2. *Resonant triad interactions*

We have searched for and located numerous examples of Craik-type resonant triads (Craik 1971), for various values of α, R and of the wall parameters m, c_0, d, S. The located triads comprise a variety of combinations of TS, F and HO modes. Triads composed of three TS waves show non-trivial but small differences from rigid-wall analogues regarding both the magnitudes of the quadratic interaction coefficients a_3 and a_1 and their respective variations with α and R. It has been demonstrated that triads of three wall modes (that is, F modes) are possible for our spring-backed tension-membrane wall model. These triads are not found at such low values of α as TS triads, because of differences in the α-variation of c_r and $\tilde{c}_r$. Meaningful comparison of quadratic interaction coefficients for wall-mode triads with those for TS triads is not easy because of the difficulty in defining a mutually satisfactory normalization of the respective eigenfunctions.

Triads comprising a streamwise TS mode and two oblique (strongly linearly damped) HO modes have been found for both rigid- and compliant-wall cases. These are notable principally for the remarkably large magnitudes of the quadratic interaction coefficients: $|a_1| \sim O(1000)$. The streamwise, reasonably near-neutral TS mode has a less exceptional interaction coefficient, though: $|a_3| \sim O(1)$. It is known (Mack 1976) that for HO modes c_i approaches zero with increasing α or R (as does c_r), implying that such resonant-triad interactions may well be of physical significance at large wavenumbers. Large values of R are of course unlikely to be practically important however, as they imply turbulent flow regimes.

It appears that Squire modes can greatly affect the strength of resonant triad interactions at quadratic order, if the real parts of the phase speeds of the Squire mode and one of the resonant modes are very close. In conclusion, it is clear that flexible walls greatly enrich the possibilities for the formation of resonant triads, but linear instabilities in the form of modal interactions tend often to be present for the required parameter values. The strength of these often vigorous instabilities can be reduced by the introduction of judicious amounts of wall damping, but this tends to further complicate the phenomenology of the interactions.

The majority of this work was performed whilst the author was in receipt of an SERC(CASE) studentship at the University of St. Andrews, supervised by Professor

A. D. D. Craik, to whom the author is most grateful. Thanks are also due to Professor P. K. Sen of the Indian Institute of Technology, Delhi, for instruction in computational methods during a three-month visit of the author to Delhi in 1988, to the IIT authorities for providing a visiting research scholarship, and to the Procurement Executive, Ministry of Defence for meeting some of the travel costs. The work was completed while the author was in receipt of a SERC research grant at the University of Exeter.

REFERENCES

BENJAMIN, T. B. 1963 The threefold classification of unstable disturbances in flexible surfaces bounding inviscid flows. *J. Fluid Mech.* **16**, 436–450.

CAIRNS, R. A. 1979 The role of negative energy waves in some instabilities of parallel flows. *J. Fluid Mech.* **92**, 1–14.

CARPENTER, P. W. 1990 Status of transition delay using compliant walls. In *Viscous Drag Reduction* (ed. D. M. Bushnell & J. N. Heffner). *Progress in Astronautics and Aeronautics*, vol. 123. AIAA.

CARPENTER, P. W. & GAJJAR, J. S. B. 1990 A general theory for two- and three-dimensional wall-mode instabilities in boundary layers over isotropic and anisotropic compliant walls. *Theor. Comput. Fluid Dyn.* **1**, 349–378.

CARPENTER, P. W. & GARRAD, A. D. 1985 The hydrodynamic stability of flow over Kramer-type compliant surfaces. Part 1. Tollmien–Schlichting instabilities. *J. Fluid Mech.* **155**, 465–510.

CARPENTER, P. W. & GARRAD, A. D. 1986 The hydrodynamic stability of flow over Kramer-type compliant surfaces. Part 2. Flow-induced surface instabilities. *J. Fluid Mech.* **170**, 199–232.

CARPENTER, P. W. & MORRIS, P. J. 1990 The effect of anisotropic wall compliance on boundary-layer stability and transition. *J. Fluid Mech.* **218**, 171–223.

CORNER, D., HOUSTON, D. J. R. & ROSS, M. A. S. 1976 Higher eigenstates in boundary-layer stability theory. *J. Fluid Mech.* **77**, 81–103.

CRAIK, A. D. D. 1971 Non-linear resonant instability in boundary layers. *J. Fluid Mech.* **50**, 393–413.

CRAIK, A. D. D. 1985 *Wave Interactions And Fluid Flows*. Cambridge University Press.

CRAIK, A. D. D. & ADAM, J. A. 1979 'Explosive' resonant wave interactions in a three-layer fluid flow. *J. Fluid Mech.* **92**, 15–33.

DAVEY, A. & REID, W. H. 1977 On the stability of stratified viscous plane Couette flow. Part 1. Constant buoyancy flow. *J. Fluid Mech.* **80**, 509–525.

DOMARADZKI, J. & METCALFE, R. W. 1987 Stabilization of laminar boundary layers by compliant membranes. *Phys. Fluids* **30**, 695–705.

GAD-EL-HAK, M., BLACKWELDER, R. F. & RILEY, J. J. 1984 On the interaction of compliant coatings with boundary-layer flows. *J. Fluid Mech.* **140**, 257–280.

GILL, A. E. & DAVEY, A. 1969 Instabilities of a buoyancy-driven system. *J. Fluid Mech.* **35**, 775–798.

GUSTAVSSON, L. H. 1981 Resonant growth of three-dimensional disturbances in plane Poiseuille flow. *J. Fluid Mech.* **112**, 253–264.

GUSTAVSSON, L. H. & HULTGREN, L. S. 1980 A resonance mechanism in plane Couette flow. *J. Fluid Mech.* **98**, 149–159.

HERBERT, T. 1983 Subharmonic three-dimensional disturbances in unstable shear flows. *AIAA Paper* 83–1759.

HERBERT, T. 1988 Secondary instability in boundary layers. *Ann. Rev. Fluid Mech.* **20**, 487–526.

HULTGREN, L. S. & GUSTAVSSON, L. H. 1981 Algebraic growth of disturbances in a laminar boundary layer. *Phys. Fluids* **24**, 1000–1004.

INCE, E. L. 1956 *Ordinary Differential Equations*. Dover.

ITOH, N. 1974 Spatial growth of finite wave disturbances in parallel and nearly parallel flows. Part 1. The theoretical analysis and the numerical results for plane Poiseuille flow. *Trans. Japan Soc. Aero. Space Sci.* **17**, 160–174.

JOSEPH, D. D. 1968 Eigenvalue bounds for the Orr–Sommerfeld equation. *J. Fluid Mech.* **33**, 617–621.

JOSEPH, D. D. 1969 Eigenvalue bounds for the Orr–Sommerfeld equation. Part 2. *J. Fluid Mech.* **36**, 721–734.

KACHANOV, YU. S. & LEVCHENKO, YA. V. 1984 The resonant interaction of disturbances at laminar-turbulent transition in a boundary layer. *J. Fluid Mech.* **138**, 209–247.

LANDAHL, M. T. 1962 On the stability of a laminar incompressible boundary layer over a flexible surface *J. Fluid Mech.* **13**, 609–632.

MACK, L. M. 1976 A numerical study of the temporal eigenvalue spectrum of the Blasius boundary layer. *J. Fluid Mech.* **73**, 497–520.

MACK, L. M. 1984 Boundary-layer stability theory. *AGARD Special Course on Stability and Transition of Laminar Flow.*

MURDOCK, J. W. & STEWARTSON, K. 1977 Spectrum of the Orr–Somerfeld equation. *Phys. Fluids* **20**, 1404–1411.

NAYFEH, A. H. 1985 Three-dimensional spatial secondary instability in boundary-layer flows. *AIAA Paper* 85–1697.

RAETZ, G. S. 1959 A new theory of the cause of transition in fluid flows. *Norair Rep.* NOR-59–383.

ROTENBERRY, J. M. & SAFFMAN, P. G. 1990 Effect of compliant boundaries on weakly nonlinear shear waves in channel flow. *SIAM J. Appl. Maths* **50**, 261–394.

SARIC, W. S. & THOMAS, A. S. W. 1984 Experiments on the subharmonic route to turbulence in boundary layers. *Proc. IUTAM Symp. on Turbulent and Chaotic Phenomena in Fluids, Kyoto, Japan, Sept. 1983.*

SEN, P. K. & ARORA, D. S. 1988 On the stability of laminar boundary-layer flow over a flat-plane with a compliant surface. *J. Fluid Mech.* **197**, 201–240.

SMITH, F. T. 1979 On the non-parallel flow stability of the Blasius boundary layer. *Proc. R. Soc. Lond.* A **366**, 91–109.

SMITH, F. T. & STEWART, P. A. 1987 The resonant-triad nonlinear interaction in boundary-layer transition. *J. Fluid Mech.* **179**, 227–252.

SQUIRE, H. B. 1933 On the stability for three-dimensional disturbances of viscous fluid flow between parallel walls. *Proc. R. Soc. Lond.* A **142**, 621–628.

THOMAS, L. H. 1953 The stability of plane Poiseuille flow. *Phys. Rev.* **91**, 780–784.

THOMAS, M. D. & CRAIK, A. D. D. 1988 Three-wave resonance for free-surface flows over flexible boundaries. *J. Fluids Struct.* **2**, 323–338.

USHER, J. R. & CRAIK, A. D. D. 1974 Nonlinear wave interactions in shear flows. Part 1. A variational formulation. *J. Fluid Mech.* **66**, 209–221.

USHER, J. R. & CRAIK, A. D. D. 1975 Nonlinear wave interactions in shear flows. Part 2. Third-order theory. *J. Fluid Mech.* **70**, 437–461.

VOLODIN, A. G. & ZEL'MAN, M. B. 1979 Three-wave resonance interaction of disturbances in a boundary layer. *Fluid Dyn.* **13**, 698–703. [translation of *Mekh. Zhid. i Gaza* **5**, 78–84].

WILLIS, G. J. K. 1986 Hydrodynamic stability of boundary layers over compliant surfaces. Ph.D. thesis, University of Exeter.

YEO, K. S. 1986 The stability of flow over flexible surfaces. Ph.D. thesis, University of Cambridge.